CP Violation and Flavour Mixing in the Standard Model – 1996 Update

A. Ali[a], D. London[b]

[a] Deutsches Elektronen-Synchrotron DESY, Notkestrasse 85, D-22603 Hamburg, FRG
[b] Laboratoire de physique nucléaire, Université de Montréal, C.P. 6128, succ. centre-ville, Montréal, QC, Canada H3C 3J7.

Abstract: We have recently reviewed and updated the constraints on the parameters of the quark flavour mixing matrix V_{CKM} in the standard model. A summary of the main results is given here, emphasizing the features relevant for HERA-B. These include the standard model predictions for the B_s^0-$\overline{B_s^0}$ mixing parameter x_s (or, equivalently, ΔM_s) and the quantities $\sin 2\alpha$, $\sin 2\beta$ and $\sin^2\gamma$, which characterize CP asymmetries in B-decays.

1 An Update of the CKM Matrix

We have recently revised and updated the profile of the Cabibbo-Kobayashi-Maskawa (CKM) matrix [1] in Ref. [2]. Our main focus is on the CKM unitarity triangle and CP asymmetries in B decays, which are the principal objects of interest in experiments at present and forthcoming B facilities. In performing this update, we have included the improvements reported in a number of measurements of the lifetime, mixing ratio, and the CKM matrix elements $|V_{cb}|$ and $|V_{ub}/V_{cb}|$ from B decays, as well as the top quark mass, $|\epsilon|$, and progress in theoretical calculations involving a number of perturbative and non-perturbative aspects of QCD. We summarize the input and those results which have a direct bearing on the physics of HERA-B. For details and references, we refer to [2].

In updating the CKM matrix elements, we make use of the Wolfenstein parametrization [3], which follows from the observation that the elements of this matrix exhibit a hierarchy in terms of λ, the Cabibbo angle. In this parametrization the CKM matrix can be written approximately as

$$V_{CKM} \simeq \begin{pmatrix} 1-\frac{1}{2}\lambda^2 & \lambda & A\lambda^3(\rho - i\eta) \\ -\lambda(1+iA^2\lambda^4\eta) & 1-\frac{1}{2}\lambda^2 & A\lambda^2 \\ A\lambda^3(1-\rho-i\eta) & -A\lambda^2 & 1 \end{pmatrix} . \quad (1)$$

We shall discuss those quantities which constrain these CKM parameters, pointing out the significant input in the determination of λ, A, ρ and η.

- $|V_{us}|$: We recall that $|V_{us}|$ has been extracted with good accuracy from $K \to \pi e \nu$ and hyperon decays [4] to be

$$|V_{us}| = \lambda = 0.2205 \pm 0.0018 \ . \tag{2}$$

This agrees quite well with the determination of $V_{ud} \simeq 1 - \frac{1}{2}\lambda^2$ from β-decay [4],

$$|V_{ud}| = 0.9736 \pm 0.0010 \ . \tag{3}$$

- $|V_{cb}|$: The determination of $|V_{cb}|$ from inclusive and exclusive B decays has been reviewed earlier in a number of studies [5, 6, 7, 8]. Here, we shall concentrate on the exclusive decay $B \to D^* \ell \nu_\ell$ analyzed in the context of heavy quark effective theory (HQET) [9], as this method seems to have been scrutinized in great detail. This gives [2]:

$$|V_{cb}| = 0.0393 \pm 0.0028 \ , \tag{4}$$

yielding

$$A = 0.81 \pm 0.058 \ . \tag{5}$$

- $|V_{ub}/V_{cb}|$: The knowledge of the CKM matrix element ratio $|V_{ub}/V_{cb}|$ is based on the analysis of the end-point lepton energy spectrum in semileptonic decays $B \to X_u \ell \nu_\ell$ and the measurement of the exclusive semileptonic decays $B \to (\pi, \rho) \ell \nu_\ell$ reported by the CLEO collaboration [8]. Present measurements in both the inclusive and exclusive modes are compatible with [10]:

$$\left| \frac{V_{ub}}{V_{cb}} \right| = 0.08 \pm 20\% \ . \tag{6}$$

This gives

$$\sqrt{\rho^2 + \eta^2} = 0.363 \pm 0.073 \ . \tag{7}$$

- $|\epsilon|, \hat{B}_K,$ and constraints on ρ and η: The experimental value of $|\epsilon|$ is [4]:

$$|\epsilon| = (2.280 \pm 0.013) \times 10^{-3} \ . \tag{8}$$

Theoretically, $|\epsilon|$ is essentially proportional to the imaginary part of the box diagram for K^0-$\overline{K^0}$ mixing and is given by [11]

$$\begin{aligned} |\epsilon| = \frac{G_F^2 f_K^2 M_K M_W^2}{6\sqrt{2}\pi^2 \Delta M_K} \hat{B}_K \left(A^2 \lambda^6 \eta \right) & \left(y_c \left\{ \hat{\eta}_{ct} f_3(y_c, y_t) - \hat{\eta}_{cc} \right\} \right. \\ & \left. + \ \hat{\eta}_{tt} y_t f_2(y_t) A^2 \lambda^4 (1-\rho) \right), \end{aligned} \tag{9}$$

where $y_i \equiv m_i^2/M_W^2$, and the functions f_2 and f_3 can be found in Ref. [5]. Here, the $\hat{\eta}_i$ are QCD correction factors, calculated at next-to-leading order in [12] ($\hat{\eta}_{cc}$), [13] ($\hat{\eta}_{tt}$) and [14] ($\hat{\eta}_{ct}$). The theoretical uncertainty in the expression for $|\epsilon|$ is in the renormalization-scale independent parameter $\hat{B}_K$, which represents our ignorance of the hadronic matrix element $\langle K^0 | (\overline{d} \gamma^\mu (1-\gamma_5) s)^2 | \overline{K^0} \rangle$. Recent calculations of $\hat{B}_K$ using lattice QCD methods and the $1/N_c$ approach are summarized in [2], which gives

$$\hat{B}_K = 0.75 \pm 0.10. \tag{10}$$

- ΔM_d, $f^2_{B_d}\hat{B}_{B_d}$, and constraints on ρ and η: The present world average for ΔM_d is $\Delta M_d = 0.464 \pm 0.018\ (ps)^{-1}$ [10] . The mass difference ΔM_d is calculated from the B^0_d-$\overline{B^0_d}$ box diagram. Unlike the kaon system, where the contributions of both the c- and the t-quarks in the loop are important, this diagram is dominated by t-quark exchange:

$$\Delta M_d = \frac{G_F^2}{6\pi^2} M_W^2 M_B \left(f^2_{B_d}\hat{B}_{B_d}\right) \hat{\eta}_B y_t f_2(y_t) |V^*_{td}V_{tb}|^2 \ , \tag{11}$$

where, using Eq. 1, $|V^*_{td}V_{tb}|^2 = A^2\lambda^6[(1-\rho)^2+\eta^2]$. Here, $\hat{\eta}_B$ is the QCD correction. In the fits presented in [2] we used the value $\hat{\eta}_B = 0.55$, calculated in the $\overline{MS}$ scheme, following Ref. [13]. Consistency requires that the top quark mass be rescaled from its pole (mass) value of $m_t = 175 \pm 9$ GeV to the value $\overline{m_t}(m_t(pole)) = 165 \pm 9$ GeV in the $\overline{MS}$ scheme. For the B system, the hadronic uncertainty is given by $f^2_{B_d}\hat{B}_{B_d}$, analogous to $\hat{B}_K$ in the kaon system, except that in this case f_{B_d} has not been measured. In our fits in [2], we have taken

$$f_{B_d}\sqrt{\hat{B}_{B_d}} = 200 \pm 40 \text{ MeV} \ , \tag{12}$$

which is compatible with the results from both lattice-QCD and QCD sum rules for this quantity.

For the CKM fits, the present experimental input can be summarized as follows:

$$\begin{aligned} \sqrt{\rho^2+\eta^2} &= 0.363 \pm 0.073 \quad (\text{from } |V_{ub}/V_{cb}|), \\ (f_{B_d}\sqrt{\hat{B}_{B_d}}/1\ \text{GeV})\sqrt{(1-\rho)^2+\eta^2} &= 0.202 \pm 0.017 \quad (\text{from } \Delta M_d), \\ \hat{B}_K\eta[0.93 + (2.08 \pm 0.34)(1-\rho)] &= (0.79 \pm 0.11) \quad (\text{from } |\epsilon|), \end{aligned} \tag{13}$$

The errors of the last two lines include the small experimental errors on ΔM_d (3.6%) and $|\epsilon|$ (0.6%), as well as the larger errors on m_t^2 (11%) and A^2 (14%). Adding all these errors in quadrature, one finds that the total experimental errors involved in $|V_{ub}/V_{cb}|$, ΔM_d and $|\epsilon|$ are about 20%, 8% and 16%, respectively. The theoretical error on $f_{B_d}\sqrt{\hat{B}_{B_d}}$ is about 20% and on $\hat{B}_K$ about 13%. Thus, one sees that the present theoretical and experimental errors are not terribly different.

We have considered two types of fits in Ref. [2]. In Fit 1, we assume particular fixed values for the theoretical hadronic quantities. The allowed ranges for the CKM parameters are derived from the (Gaussian) errors on experimental measurements only. In Fit 2, we assign a central value plus an error (treated as Gaussian) to the theoretical quantities. In the resulting fits, we combine the experimental and theoretical errors in quadrature. For both fits we calculate the allowed region in CKM parameter space at 95% C.L.

We have also estimated in [2] the SM prediction for the B^0_s-$\overline{B^0_s}$ mixing parameter, ΔM_s and x_s. The experimental lower limits on these quantities have steadily increased, thanks to the experiments at LEP [16, 17] and more recently also from SLC. These limits have now started to be significant for the allowed CKM parameter space. We show how the improved ALEPH limit of $\Delta M_s > 7.8\ (\text{ps})^{-1}$ leading to $\Delta M_s/\Delta M_d > 16.0$ (95% C.L.) [15, 17] constrains the CKM parameter space. We have presented in [2] the allowed ranges for the CP-violating phases that

Parameter	Value
λ	0.2205
$\lvert V_{cb}\rvert$	0.0393 ± 0.0028
$\lvert V_{ub}/V_{cb}\rvert$	0.08 ± 0.016
$\lvert\epsilon\rvert$	$(2.280 \pm 0.013) \times 10^{-3}$
ΔM_d	$(0.464 \pm 0.018)\ (ps)^{-1}$
$\tau(B_d)$	$(1.52 \pm 0.05)\ (ps)$
$\overline{m_t}(m_t(pole))$	(165 ± 9) GeV
$\hat{\eta}_B$	0.55
$\hat{\eta}_{cc}$	1.38
$\hat{\eta}_{ct}$	0.47
$\hat{\eta}_{tt}$	0.57
$\hat{B}_K$	0.75 ± 0.1
$f_{B_d}\sqrt{\hat{B}_{B_d}}$	200 ± 40 MeV

Table 1: Parameters used in the CKM fits. Values of the hadronic quantities $\hat{B}_K$ and $f_{B_d}\sqrt{\hat{B}_{B_d}}$ shown are motivated by lattice QCD results, QCD sum rules and chiral perturbation theory. In Fit 1, specific values of these hadronic quantities are chosen, while in Fit 2, they are allowed to vary over the given ranges.

will be measured in B decays, characterized by $\sin 2\beta$, $\sin 2\alpha$ and $\sin^2\gamma$. These can be measured directly through rate asymmetries in the decays $\overset{(-)}{B_d} \to J/\psi K_S$, $\overset{(-)}{B_d} \to \pi^+\pi^-$, and $\overset{(-)}{B_s} \to D_s^{\pm} K^{\mp}$ (or $B^{\pm} \to \overset{(-)}{D} K^{\pm}$), respectively. We also show the allowed correlated domains for two of the CP asymmetries $(\sin 2\alpha, \sin 2\beta)$.

This contribution is organized as follows. In Section 2, we summarize the results of our updated fits for the CKM parameters [2] in terms of the allowed domains of the unitarity triangle, which are displayed in several figures and tables. In Section 3, we discuss the impact of the recent lower limit on the ratio $\Delta M_s/\Delta M_d$ reported by the ALEPH collaboration on the CKM parameters and estimate the expected range of the mixing ratio x_s and ΔM_s in the SM based on our fits. In Section 4 we discuss the predictions for the CP asymmetries in the neutral B meson sector and calculate the correlations for the CP-violating asymmetries proportional to $\sin 2\alpha$, $\sin 2\beta$ and $\sin^2\gamma$. Section 5 contains a summary and an outlook for improving the profile of the CKM unitarity triangle.

2 The Unitarity Triangle

The allowed region in ρ-η space can be displayed quite elegantly using the so-called unitarity triangle. The unitarity of the CKM matrix leads to the following relation:

$$V_{ud}V_{ub}^* + V_{cd}V_{cb}^* + V_{td}V_{tb}^* = 0 \ . \tag{14}$$

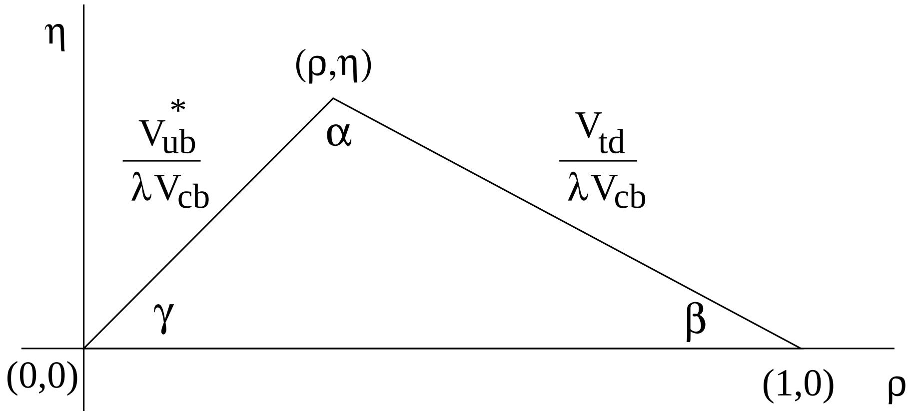

Figure 1: The unitarity triangle. The angles α, β and γ can be measured via CP violation in the B system.

Using the form of the CKM matrix in Eq. 1, this can be recast as

$$\frac{V_{ub}^*}{\lambda V_{cb}} + \frac{V_{td}}{\lambda V_{cb}} = 1 \ , \tag{15}$$

which is a triangle relation in the complex plane (i.e. ρ-η space), illustrated in Fig. 1. Thus, allowed values of ρ and η translate into allowed shapes of the unitarity triangle.

In order to find the allowed unitarity triangles, the computer program MINUIT is used to fit the CKM parameters A, ρ and η to the experimental values of $|V_{cb}|$, $|V_{ub}/V_{cb}|$, $|\epsilon|$ and x_d. Since λ is very well measured, we have fixed it to its central value given above. As discussed in the introduction, two types of fits have been presented in [2]. We first discuss the "experimental fit" (Fit 1). The goal here is to restrict the allowed range of the parameters (ρ, η) for given values of the coupling constants $f_{B_d}\sqrt{\hat{B}_{B_d}}$ and $\hat{B}_K$. For each value of $\hat{B}_K$ and $f_{B_d}\sqrt{\hat{B}_{B_d}}$, the CKM parameters A, ρ and η are fit to the experimental numbers given in Table 1 and the χ^2 is calculated.

First, we fix $\hat{B}_K = 0.75$, and vary $f_{B_d}\sqrt{\hat{B}_{B_d}}$ in the range 130 MeV to 240 MeV. The resulting χ^2_{min} values were calculated together with the best-fit values of the CKM parameters (ρ, η), which can be seen in [2]. The fits are presented as an allowed region in ρ-η space at 95% C.L. ($\chi^2 = \chi^2_{min} + 6.0$). The results are shown in Fig. 2. As we pass from Fig. 2 (top left) to Fig. 2 (bottom right), the unitarity triangles represented by these graphs become more and more obtuse, which leads us to the conclusion that our quantitative knowledge of the unitarity triangle is at present not very solid. This is seen more clearly in the results of Fit 2. So, unless our knowledge of hadronic matrix elements improves considerably, measurements of $|\epsilon|$ and x_d, no matter how precise, will not help much in further constraining the unitarity triangle. This is why measurements of CP-violating rate asymmetries in the B system are so important [19, 20]. Being largely independent of theoretical uncertainties, they will allow us to accurately pin down the unitarity triangle.

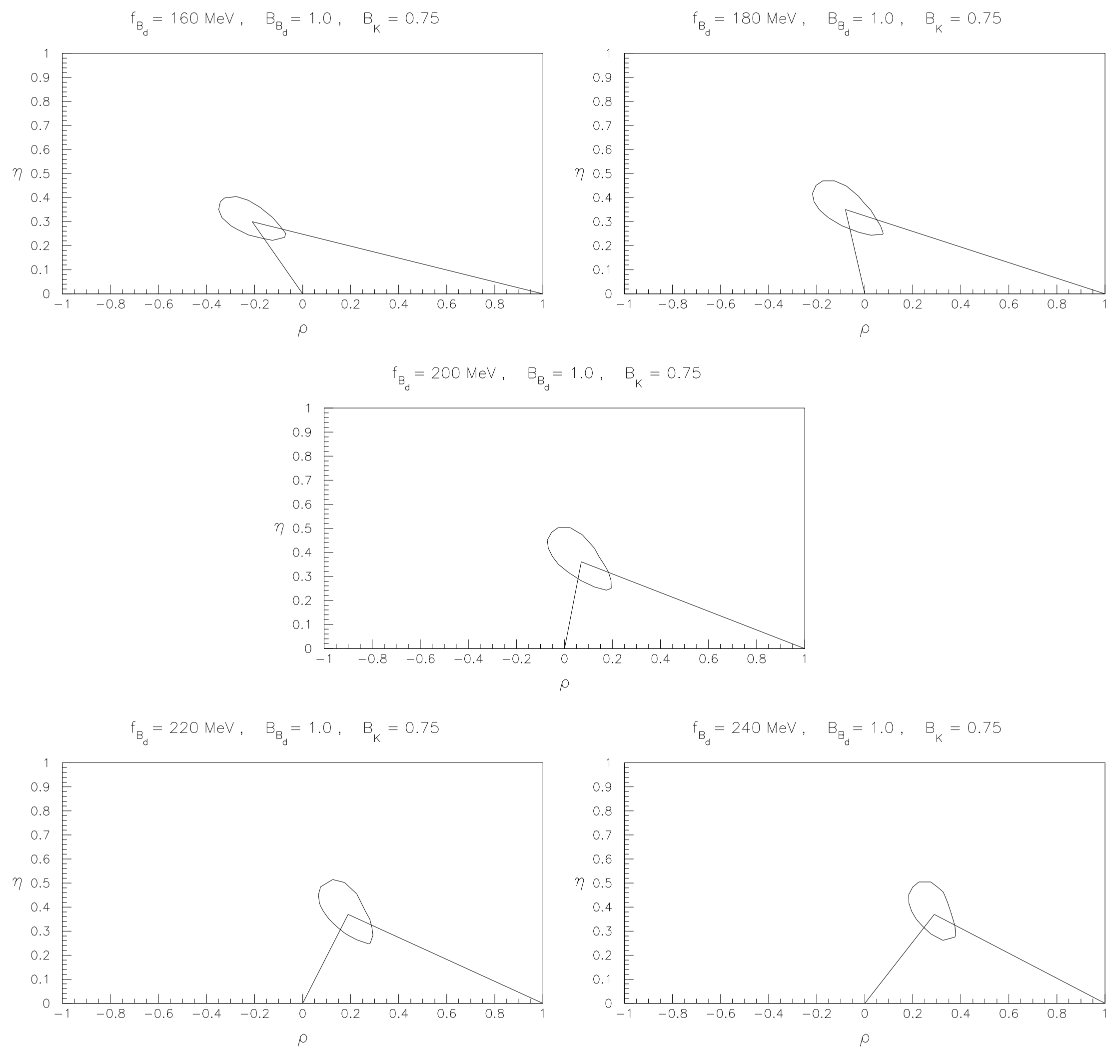

Figure 2: Allowed region in ρ-η space, from a fit to the experimental values given in Table 1. We have fixed $\hat{B}_K = 0.75$ and vary the coupling constant product $f_{B_d}\sqrt{\hat{B}_{B_d}}$ as indicated on the figures. The solid line represents the region with $\chi^2 = \chi^2_{min} + 6$ corresponding to the 95% C.L. region. The triangles show the best fit.

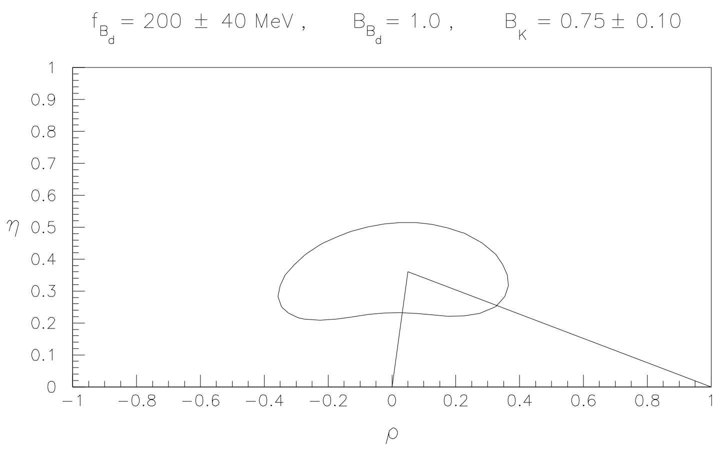

Figure 3: Allowed region in ρ-η space, from a simultaneous fit to both the experimental and theoretical quantities given in Table 1. The theoretical errors are treated as Gaussian for this fit. The solid line represents the region with $\chi^2 = \chi^2_{min} + 6$ corresponding to the 95% C.L. region. The triangle shows the best fit.

We now discuss the "combined fit" (Fit 2). Since the coupling constants are not known and the best we have are estimates given in the ranges in Eqs. (10) and (12), a reasonable profile of the unitarity triangle at present can be obtained by letting the coupling constants vary in these ranges. The resulting CKM triangle region is shown in Fig. 3. As is clear from this figure, the allowed region is still rather large at present. However, present data and theory do restrict the parameters ρ and η to lie in the following range:

$$\begin{aligned} 0.20 \leq \eta \leq 0.52, \\ -0.35 \leq \rho \leq 0.35 \ . \end{aligned} \tag{16}$$

The preferred values obtained from the "combined fit" are

$$(\rho, \eta) = (0.05, 0.36) \quad (\text{with } \chi^2 = 6.6 \times 10^{-3}) \ , \tag{17}$$

which gives rise to an almost right-angled unitarity triangle, with the angle γ being close to 90 degrees. However, as we quantify below, the allowed ranges of the CP violating angles α, β, and γ estimated at the 95% C.L. are still quite large, though correlated.

Finally, to check that our combined fit (Fit 2) is not introducing a significant theoretical bias in estimating the profile of the unitarity triangle, we have also determined the allowed parameter space in the ρ–η plane by overlaying the individual constraints following from the experimental measurements of $|V_{ub}/V_{cb}|$, $|\epsilon|$, and ΔM_d given in Eqs. (13). In doing this, we took the central experimental value for the ratio $|V_{ub}/V_{cb}|$, and varied the experimental error by $\pm 2\sigma$, which is then a common feature with Fit 2. For $|\epsilon|$ and ΔM_d, we varied the experimental errors by $\pm 1\sigma$ and varied the theoretical input $\hat{B}_K$ in the range $0.65 \leq \hat{B}_K \leq 0.85$ and $f_{B_d}\sqrt{\hat{B}_{B_d}}$ in the range 160 MeV $\leq f_{B_d}\sqrt{\hat{B}_{B_d}} \leq$ 240 MeV. The resulting allowed domain in the ρ–η plane is shown in Fig. 4 together with the (95%) C.L. contours allowed by our Fit 2. This plot shows that one gets essentially the same allowed region using the two techniques, reflecting the fact

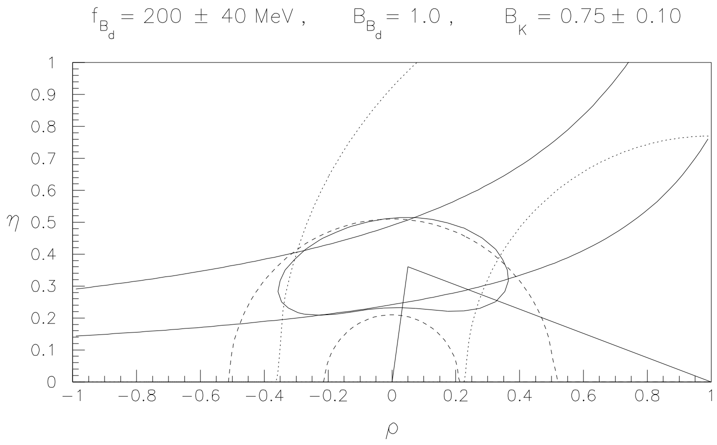

Figure 4: Allowed region in ρ-η space obtained by overlaying the individual constraints following from $|V_{ub}/V_{cb}|$ (with $\pm 2\sigma$ error) (dashed curves), $|\epsilon|$ (solid curves), and ΔM_d (dotted curves) [both with $\pm 1\sigma$ errors given in Eqs. (13)], and varying $\hat{B}_K$ in the range $0.65 \leq \hat{B}_K \leq 0.85$ and $f_{B_d}\sqrt{\hat{B}_{B_d}}$ in the range 160 MeV $\leq f_{B_d}\sqrt{\hat{B}_{B_d}} \leq$ 240 MeV. The 95% C.L. contour from Fig. 3 resulting from a simultaneous fit to both the experimental and theoretical quantities in Table 1 is also shown ("haggis"-type curve). The triangle shows the best fit.

that the experimental and theoretical errors at present are very similar. In view of this, we shall now show only results from our Fit 2.

3 ΔM_s (and x_s) and the Unitarity Triangle

Mixing in the B_s^0-$\overline{B_s^0}$ system is quite similar to that in the B_d^0-$\overline{B_d^0}$ system. The B_s^0-$\overline{B_s^0}$ box diagram is again dominated by t-quark exchange, and the mass difference between the mass eigenstates ΔM_s is given by a formula analogous to that of Eq. (11):

$$\Delta M_s = \frac{G_F^2}{6\pi^2} M_W^2 M_{B_s} \left(f_{B_s}^2 \hat{B}_{B_s} \right) \hat{\eta}_{B_s} y_t f_2(y_t) |V_{ts}^* V_{tb}|^2 \ . \tag{18}$$

Using the fact that $|V_{cb}| = |V_{ts}|$ (Eq. 1), it is clear that one of the sides of the unitarity triangle, $|V_{td}/\lambda V_{cb}|$, can be obtained from the ratio of ΔM_d and ΔM_s,

$$\frac{\Delta M_s}{\Delta M_d} = \frac{\hat{\eta}_{B_s} M_{B_s} \left(f_{B_s}^2 \hat{B}_{B_s} \right)}{\hat{\eta}_{B_d} M_{B_d} \left(f_{B_d}^2 \hat{B}_{B_d} \right)} \left| \frac{V_{ts}}{V_{td}} \right|^2 . \tag{19}$$

All dependence on the t-quark mass drops out, leaving the square of the ratio of CKM matrix elements, multiplied by a factor which reflects $SU(3)_{\mathrm{flavour}}$ breaking effects. The only real uncertainty in this factor is the ratio of hadronic matrix elements. Whether or not x_s can be used to help constrain the unitarity triangle will depend crucially on the theoretical status of the ratio $f_{B_s}^2 \hat{B}_{B_s}/f_{B_d}^2 \hat{B}_{B_d}$. In what follows, we will take $\xi_s \equiv (f_{B_s}\sqrt{\hat{B}_{B_s}})/(f_{B_d}\sqrt{\hat{B}_{B_d}}) = (1.15 \pm 0.05)$, consistent with both lattice-QCD [21] and QCD sum rules [22]. (The SU(3)-breaking factor in $\Delta M_s/\Delta M_d$ is ξ_s^2.)

The mass and lifetime of the B_s meson have now been measured at LEP and Tevatron and their present values are $M_{B_s} = 5369.3 \pm 2.0$ MeV and $\tau(B_s) = 1.52 \pm 0.07$ ps [23]. The QCD correction factor $\hat{\eta}_{B_s}$ is equal to its B_d counterpart, i.e. $\hat{\eta}_{B_s} = 0.55$. The main uncertainty in ΔM_s (or, equivalently, x_s) is now $f_{B_s}^2 \hat{B}_{B_s}$. Using the determination of A given previously, $\tau_{B_s} = 1.52 \pm 0.07$ (ps) and $\overline{m_t} = 165 \pm 9$ GeV, we obtain [2]:

$$\begin{aligned} \Delta M_s &= (12.8 \pm 2.1) \frac{f_{B_s}^2 \hat{B}_{B_s}}{(230 \text{ MeV})^2} \, (ps)^{-1} \ , \\ x_s &= (19.5 \pm 3.3) \frac{f_{B_s}^2 \hat{B}_{B_s}}{(230 \text{ MeV})^2} \ . \end{aligned} \tag{20}$$

The choice $f_{B_s}\sqrt{\hat{B}_{B_s}} = 230$ MeV corresponds to the central value given by the lattice-QCD estimates, and with this our fits give $x_s \simeq 20$ as the preferred value in the SM. Allowing the coefficient to vary by $\pm 2\sigma$, and taking the central value for $f_{B_s}\sqrt{\hat{B}_{B_s}}$, this gives

$$\begin{aligned} 12.9 \leq x_s \leq 26.1 \ , \\ 8.6 \, (ps)^{-1} \leq \Delta M_s \leq 17.0 \, (ps)^{-1} \ . \end{aligned} \tag{21}$$

It is difficult to ascribe a confidence level to this range due to the dependence on the unknown coupling constant factor. All one can say is that the standard model predicts large values for ΔM_s (and hence x_s), which are somewhat above the present experimental limit $\Delta M_s > 9.2 \, (ps)^{-1}$ [10, 17].

Summarizing the discussion on x_s, we note that the lattice-QCD-inspired estimate $f_{B_s}\sqrt{\hat{B}_{B_s}} \simeq 230$ MeV and the CKM fit predict that x_s lies between 13 and 26, with a central value around 20. All of these values scale as $(f_{B_s}\sqrt{\hat{B}_{B_s}}/230 \text{ MeV})^2$. The present constraints from the lower bound on ΔM_s on the CKM parameters are now competitive with those from fits to other data. In particular, the LEP-bound $\Delta M_s/\Delta M_d > 19.0$ removes the large-negative-ρ region, leaving the reduced range $[-0.25 \leq \rho \leq 0.35, \ 0.25 \leq \eta \leq 0.52]$ as the allowed one [2]. This is shown in Fig. 5. The constraints on the unitarity triangle from ΔM_s will become more pronounced with improved data. At HERA-B, one expects to reach a sensitivity $x_s \simeq 17$ (or $\Delta M_s \simeq 11 \, ps^{-1}$) combining various tagging techniques and data for three years [18]. Of course, an actual measurement of ΔM_s (equivalently x_s) would be very helpful in further constraining the CKM parameter space.

4 CP Violation in the B System

It is expected that the B system will exhibit large CP-violating effects, characterized by nonzero values of the angles α, β and γ in the unitarity triangle (Fig. 1) [19]. The most promising method to measure CP violation is to look for an asymmetry between $\Gamma(B^0 \to f)$ and $\Gamma(\overline{B^0} \to f)$, where f is a CP eigenstate. If only one weak amplitude contributes to the decay, the CKM phases

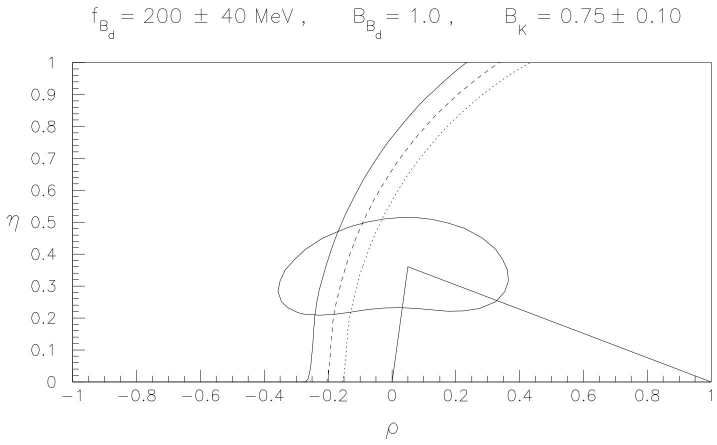

Figure 5: Further constraints in ρ-η space from the LEP bound $\Delta M_s/\Delta M_d > 19.0$. The bounds are presented for 3 choices of the SU(3)-breaking parameter: $\xi_s^2 = 1.21$ (dotted line), 1.32 (dashed line) and 1.44 (solid line). In all cases, the region to the left of the curve is ruled out.

can be extracted cleanly (i.e. with no hadronic uncertainties). Thus, $\sin 2\alpha$ and $\sin 2\beta$ can in principle be measured in $\overset{(-)}{B_d} \to \pi^+\pi^-$ and $\overset{(-)}{B_d} \to J/\psi K_S$, respectively. Penguin diagrams [24] may introduce some hadronic uncertainty into the measurement of $\sin 2\alpha$, but this can be removed via an isospin analysis [25]. For the measurement of the angle γ, two other methods have been devised, not involving CP-eigenstate final states. The CP asymmetry in the decay $\overset{(-)}{B_s} \to D_s^\pm K^\mp$ can be used to extract $\sin^2\gamma$ [26]. Similarly, the CP asymmetry in $B^\pm \to D^0_{CP} K^\pm$ also measures $\sin^2\gamma$ [27]. Here, D^0_{CP} is a D^0 or $\overline{D^0}$ which is identified in a CP-eigenstate mode (e.g. $\pi^+\pi^-$, K^+K^-, ...).

These CP-violating asymmetries can be expressed straightforwardly in terms of the CKM parameters ρ and η. The 95% C.L. constraints on ρ and η found previously can be used to predict the ranges of $\sin 2\alpha$, $\sin 2\beta$ and $\sin^2\gamma$ allowed in the standard model. The allowed ranges which correspond to each of the figures in Fig. 2, obtained from Fit 1, are found in Table 2. In this table we have assumed that the angle β is measured in $\overset{(-)}{B_d} \to J/\Psi K_S$, and have therefore included the extra minus sign due to the CP of the final state.

Since the CP asymmetries all depend on ρ and η, the ranges for $\sin 2\alpha$, $\sin 2\beta$ and $\sin^2\gamma$ shown in Table 2 are correlated. That is, not all values in the ranges are allowed simultaneously. We illustrate this in Fig. 6, corresponding to the "combined fit" (Fit 2), by showing the region in $\sin 2\alpha$-$\sin 2\beta$ space allowed by the data. From this figure one sees that the smallest value of $\sin 2\beta$ occurs in a small region of parameter space around $\sin 2\alpha \simeq 0.8$-0.9. Excluding this small tail, one expects the CP-asymmetry in $\overset{(-)}{B_d} \to J/\Psi K_S$ to be at least 20% (i.e., $\sin 2\beta > 0.4$).

5 Summary and Outlook

We summarize our results:

$f_{B_d}\sqrt{\hat{B}_{B_d}}$ (MeV)	$\sin 2\alpha$	$\sin 2\beta$	$\sin^2\gamma$
160	0.86 – 1.0	0.38 – 0.58	0.47 – 0.92
180	−0.05 – 1.0	0.47 – 0.71	0.77 – 1.0
200	−0.69 – 0.90	0.53 – 0.81	0.61 – 1.0
220	−0.85 – 0.61	0.60 – 0.89	0.44 – 0.98
240	−0.90 – 0.32	0.67 – 0.94	0.34 – 0.86

Table 2: The allowed ranges for the CP asymmetries $\sin 2\alpha$, $\sin 2\beta$ and $\sin^2\gamma$, corresponding to the constraints on ρ and η shown in Fig. 2. Values of the coupling constant $f_{B_d}\sqrt{\hat{B}_{B_d}}$ are stated. We fix $\hat{B}_K = 0.75$. The range for $\sin 2\beta$ includes an additional minus sign due to the CP of the final state $J/\Psi K_S$.

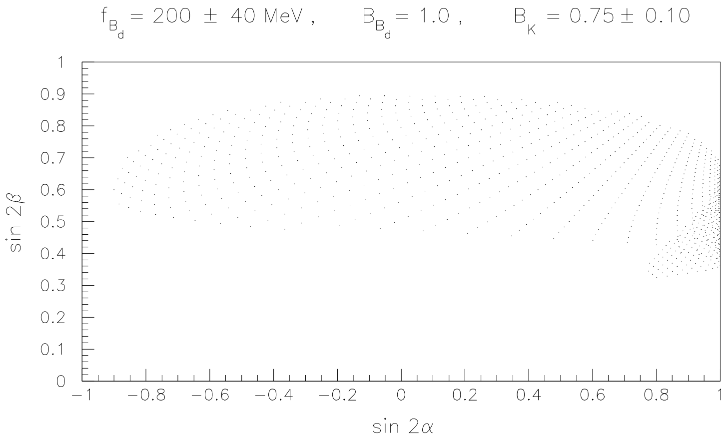

Figure 6: Allowed region of the CP-violating quantities $\sin 2\alpha$ and $\sin 2\beta$ resulting from the "combined fit" of the data for the ranges for $f_{B_d}\sqrt{\hat{B}_{B_d}}$ and $\hat{B}_K$ given in the text.

(i) We have presented an update of the CKM unitarity triangle using the theoretical and experimental improvements in the following quantities: $|\epsilon|$, $|V_{cb}|$, $|V_{ub}/V_{cb}|$, ΔM_d, $\tau(B_d)$, $\overline{m_t}$. The fits can be used to exclude extreme values of the pseudoscalar coupling constants, with the range 130 MeV $< f_{B_d}\sqrt{\hat{B}_{B_d}} <$ 250 MeV still allowed for $\hat{B}_K = 0.75$, although the fits at the two boundary values of $f_{B_d}\sqrt{\hat{B}_{B_d}}$ are poor.

(ii) The newest experimental and theoretical numbers restrict the allowed CKM unitarity triangle in the (ρ, η)-space. However, the present uncertainties are still large – despite the new, more accurate experimental data, our knowledge of the unitarity triangle is still deficient. This underscores the importance of measuring CP-violating rate asymmetries in the B system. Such asymmetries are largely independent of theoretical hadronic uncertainties, so that their measurement will allow us to accurately pin down the parameters of the CKM matrix. It may be possible to measure the parameter f_{B_d}, using isospin symmetry, via the charged-current decay $B_u^\pm \to \tau^\pm \nu_\tau$. Along the same lines, the prospects for measuring (f_{B_d}, f_{B_s}) in the FCNC leptonic and photonic decays of B_d^0 and B_s^0 hadrons, $(B_d^0, B_s^0) \to \mu^+\mu^-, (B_d^0, B_s^0) \to \gamma\gamma$ in future B physics facilities are not entirely dismal [28].

(iii) We have determined bounds on the ratio $|V_{td}/V_{ts}|$ from our fits. For 130 MeV $\leq f_{B_d}\sqrt{\hat{B}_{B_d}} \leq$ 250 MeV, i.e. in the entire allowed domain, at 95 % C.L. we find [2]

$$0.15 \leq \left|\frac{V_{td}}{V_{ts}}\right| \leq 0.34 \ . \tag{22}$$

The upper bound from this analysis is more restrictive than the current experimental upper limit following from the CKM-suppressed radiative penguin decays $BR(B \to \omega + \gamma)$ and $BR(B \to \rho + \gamma)$, which at present yield at 90% C.L. [29]

$$\left|\frac{V_{td}}{V_{ts}}\right| \leq 0.64 - 0.75 \ , \tag{23}$$

depending on the model used for the SU(3)-breaking in the relevant form factors [30]. Long-distance effects in the decay $B^\pm \to \rho^\pm + \gamma$ may introduce theoretical uncertainties comparable to those in the SU(3)-breaking part but the corresponding effects in the decays $B^0 \to (\rho^0, \omega) + \gamma$ are expected to be very small [31]. As emphasized in [28], we expect some of the CKM-suppressed radiative rare B decays will be measured at HERA-B and at the B factories, thereby making an essential input to the CKM unitarity physics.

(iv) Using the measured value of m_t, we find [2]:

$$x_s = (19.5 \pm 3.3)\, \frac{f_{B_s}^2 \hat{B}_{B_s}}{(230 \text{ MeV})^2} \ . \tag{24}$$

Taking $f_{B_s}\sqrt{\hat{B}_{B_s}} = 230$ (the central value of lattice-QCD estimates), and allowing the coefficient to vary by $\pm 2\sigma$, this gives

$$12.9 \leq x_s \leq 26.1 \ . \tag{25}$$

We conclude that the SM predicts large values for x_s, which lie above the ALEPH 95% C.L. lower limit of $x_s > 12.0$. Measurements of the B_s^0 - $\overline{B_s^0}$ oscillation frequency up to $x_s = 17$ are feasible at HERA-B, which lies inside the predicted range for this quantity given above.

(v) The ranges for the CP-violating rate asymmetries parametrized by $\sin 2\alpha$, $\sin 2\beta$ and and $\sin^2\gamma$ are determined at 95% C.L. to be [2]

$$\begin{aligned} -0.90 &\le \sin 2\alpha \le 1.0 \ , \\ 0.32 &\le \sin 2\beta \le 0.94 \ , \\ 0.34 &\le \sin^2\gamma \le 1.0 \ . \end{aligned} \tag{26}$$

Barring a small range in $\sin 2\alpha$, we expect $\sin 2\beta > 0.4$, with the central value around $\sin 2\beta = 0.63$, implying a CP-violating asymmetry $\mathcal{A}(J/\psi K_S) \simeq 30\%$, which augurs well for HERA-B and the B factories.

References

[1] N. Cabibbo, Phys. Rev. Lett. **10** (1963) 531; M. Kobayashi and K. Maskawa, Prog. Theor. Phys. **49** (1973) 652.

[2] A. Ali and D. London, preprint DESY 96-140, UdeM-GPP-TH-96-45, [hep-ph/9607392], to appear in the *Proc. of QCD Euroconference 96*, Montpellier, July 4-12, 1996.

[3] L. Wolfenstein, Phys. Rev. Lett. **51** (1983) 1945.

[4] R.M. Barnett et al. (Particle Data Group), Phys. Rev. **D54** (1996) 1.

[5] A. Ali and D. London, *Z. Phys.,* C65 (1995) 431, preprint DESY 95-148, UdeM-GPP-TH-95-32 [hep-ph/9508272], to appear in the *Proc. of the 6th Int. Symp. on Heavy Flavour Physics*, Pisa, June 6-9, 1995.

[6] M. Neubert, Preprint CERN-TH/95-107 [hep-ph/9505238].

[7] M. Shifman, Preprint TPI-MINN-95/15-T [hep-ph/9505289].

[8] T. Skwarnicki, preprint [hep-ph/9512395], to appear in the *Proc. of the 17th Int. Symp. on Lepton Photon Interactions*, Beijing, P.R. China, August 1995.

[9] N. Isgur and M.B. Wise, *Phys. Lett.,* B232 (1989) 113; 237 (1990) 527.

[10] L. Gibbons (CLEO Collaboration), Invited talk at the International Conference on High Energy Physics, Warsaw, ICHEP96 (1996). These results have been kindly communicated to us by Lawrence Gibbons for performing the CKM fits.

[11] A.J. Buras, W. Slominski, and H. Steger, Nucl. Phys. **B238** (1984) 529; *ibid.* **B245** (1984) 369.

[12] S. Herrlich and U. Nierste, Nucl. Phys. **B419** (1994) 292.

[13] A.J. Buras, M. Jamin and P.H. Weisz, Nucl. Phys. **B347** (1990) 491.

[14] S. Herrlich and U. Nierste, Phys. Rev. **D52** (1995) 6505.

[15] C. Zeitnitz, invited talk at the 4th International Workshop on B-Physics at Hadron Machines (BEAUTY 96), Rome, 17-21 June, 1996, and private communication.

[16] Sau Lan Wu, preprint WISC-EX-96-343 [hep-ex/9602003], to appear in the *Proc. of the 17th Int. Symp. on Lepton and Photon Interactions*, Beijing, P.R. China, August 1995.

[17] "Combined limit on the B_s^0 oscillation frequency", contributed paper by the ALEPH collaboration to the International Conference on High Energy Physics, Warsaw, ICHEP96 PA08-020 (1996).

[18] J. Thom (HERA-B Collaboration), to be published.

[19] For reviews, see, for example, Y. Nir and H.R. Quinn, in *B Decays*, edited by S. Stone (World Scientific, Singapore, 1992) 362; I. Dunietz, *ibid* 393.

[20] R. Aleksan, B. Kayser, and D. London, Phys. Rev. Lett. **B73** (1994) 18.

[21] H. Wittig, Invited talk presented at the III German-Russian Workshop on Heavy Quark Physics, Dubna, Russia, 20-22 May, 1996, [hep-ph/9606371].

[22] S. Narison, Phys. Lett. **B322** (1994) 247; S. Narison and A. Pivovarov, *ibid* **B327** (1994) 341.

[23] J. Richman, plenary talk at the International Conference on High Energy Physics, Warsaw, ICHEP96 (1996).

[24] D. London and R. Peccei, Phys. Lett. **B223** (1989) 257; B. Grinstein, Phys. Lett. **B229** (1989) 280; M. Gronau, Phys. Rev. Lett. **63** (1989) 1451, Phys. Lett. **B300** (1993) 163.

[25] M. Gronau and D. London, Phys. Rev. Lett. **65** (1990) 3381.

[26] R. Aleksan, I. Dunietz, and B. Kayser, Z. Phys. **C54** (1992) 653.

[27] M. Gronau and D. Wyler, Phys. Lett. **B265** (1991) 172. See also M. Gronau and D. London, Phys. Lett. **B253** (1991) 483; I. Dunietz, Phys. Lett. **B270** (1991) 75.

[28] A. Ali, preprint DESY 96-106 [hep-ph/9606324]; to appear in the Proceedings of the XX International Nathiagali Conference on Physics and Contemporary Needs, Bhurban, Pakistan, June 24-July 13, 1995 (Nova Science Publishers, New York, 1996).

[29] M. Ahtanas et al. (CLEO Collaboration), CLEO CONF 94-2 (1994).

[30] A. Ali, V.M. Braun and H. Simma, Z. Phys. **C63** (1994) 437; J.M. Soares, Phys. Rev. **D49** (1994) 283; S. Narison, Phys. Lett. **B327** (1994) 354.

[31] A. Ali and V.M. Braun, Phys. Lett. **B359** (1995) 223; A. Khodzhamirian, G. Stoll, and D. Wyler, Phys. Lett. **B358** (1995) 129.